High-power laser resistance of filled sandwich panel with truss cores: Ablation mechanisms and numerical simulation

Jiangtao Wang[a,b], Wu Yuan[a,b,*], Yuwen Liu[c], Hongwei Song[a,b], Chenguang Huang[a,b]

[a] Key Laboratory for Mechanics in Fluid-Solid Coupling Systems, Institute of Mechanics, Chinese Academy of Sciences, Beijing 100190, China
[b] School of Engineering Sciences, University of Chinese Academy of Sciences, Beijing 100049, China
[c] Department of Environment and Chemical Engineering, Yanshan University, Qinhuangdao, Hebei 066004, China

ARTICLE INFO

ABSTRACT

A new function of filled sandwich panel with truss core, superior high-power laser resistance, is reported. When filled with carbon powder-reinforced silicone resin composite, which is an ablative material, the panel exhibits superior high-power laser resistance to monolithic plate with equal areal density. This paper revealed the detailed mechanisms and reproduced the process with numerical simulation. FIIR, SEM-EDS, and TG/DSC analyses on the virgin filler material and ablation residues are conducted to investigate the thermo-physicochemical process of the filler material during the laser ablation. Considering pyrolysis, oxidation, and phase change in the laser ablation process, a 3D numerical model is developed by using the finite element method. The temperature field and ablation morphology obtained from the numerical model agree with those from the experiment. The ablation evolution process, pyrolysis effect, and laser resistance mechanism of the filled sandwich panels with truss cores are evaluated based on the present model.

1. Introduction

Sandwich panels with truss cores (SPTC) are widely investigated due to their high load-bearing capacity [1–3] and multifunctionality [4–7]. When filled with light-weight materials in the void space of the core, sandwich panels show excellent performances in thermal management [7–10], acoustic damping [11] and impact energy absorption [6,12–14]. A new function, in which the filled SPTC has excellent high-power continuous-wave (CW) laser resistance, has also been reported recently [15]. This finding may extend the application field of SPTC to laser damage protection.

Conventional laser protection structures are mainly in the form of multilayer shells or plates. As shown in Fig. 1(a), a typical structure is composed of the following layers: coating, insulation, radiation, loading-bearing, and sealing. The complicated multilayer structure aims at reducing the inner layer temperature of once subjected to intense heat flux. The outermost layer has a protective coating. According to thermomechanical properties, coating materials can be divided into reflection and ablation type [16–19]. By contrast, a new concept structure can be proposed based on the filled SPTC, which simultaneously considers laser resistance and load capability, as shown in Fig. 1(b). When high-power laser is irradiated on a bare SPTC, the input energy is mainly dissipated in the following three ways before the phase change temperature: (1) heat conduction in the outside facesheet, (2) heat conduction along truss members and (3) radiation from outside to inside facesheet. Given that the truss member is slim and thermal resistance effect is evident, radiation is the main source that relays heat to the inside facesheet. If filled with low-density material, the insulation effect may then further decrease the fraction of heat energy transferred to the inside facesheet. Therefore, the laser resistance can be improved by using the sandwich structures filled with low relative density core. In addition, when the outside facesheet reaches the phase change temperature, the shielding effect by ablation products reduces the laser energy absorbed by SPTC.

The open-cell truss core provides easy access to filling light-weight materials to further enhance the laser resistance of the SPTC. The preparation and performance of light-weight materials in high-temperature environment have been widely investigated [20]. Silicone resin composites are effective ablative materials [21]. A series of improved silicone rubber composites are manufactured, and their thermo-physical and ablation properties are studied [22,23]. These materials have been used in thermal protection system of planetary entry vehicles [24–26] and combustion chamber of rocket motors [27,28]. Filling the soft and elastic silicone resin composite in the void space of the truss
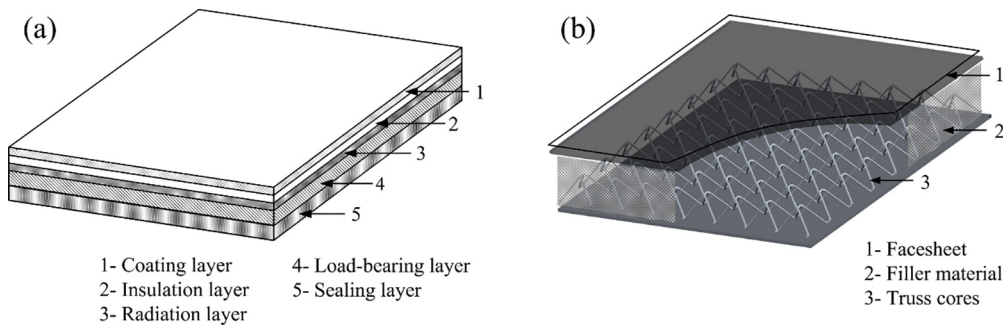
Fig. 1. Conceptional laser protection system: (a) conventional, (b) new conception.
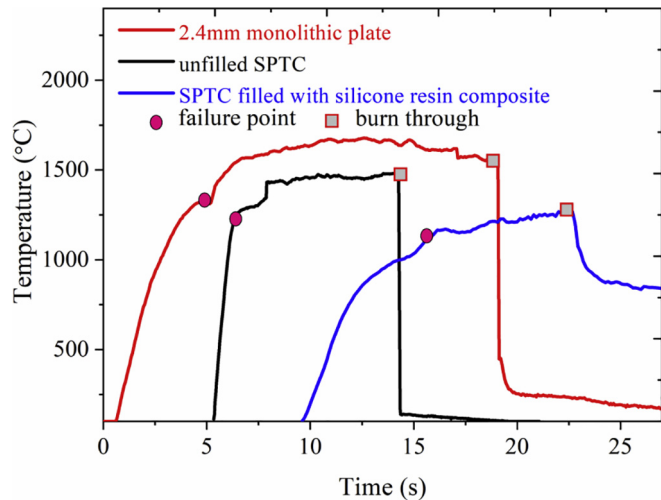

Fig. 2. Comparison of temperature histories of monolithic plate, unfilled SPTC, and SPTC with organic silicon and carbon powder.

core is easy. Experimental results indicate that filling SPTC with silicone resin composites not only delays the failure time, but also decreases the extent of ablation damage [15].

However, the detailed laser resistance mechanism of the ablative material filled SPTC and the quantitative laser ablation evolution process remains unknown. Numerical simulation of the ablation process dynamic evolution is an effective way to further understand the protective mechanism of the filled SPTC. The computing method of the ablation behavior of materials and structures used in high temperature mainly consist of volume-of-fluid (VOF) method and finite element method (FEM). VOF method is often used for C/C composites to simulate the residual fiber tip geometry and the removal of matrix [29,30]. When the thermal stress is considered, the VOF method has some limitations. A few numerical works were also conducted to simulate the ablation behavior of composite materials by using the FEM [31,32]. However, information on the FEM model for the ablation process of filled SPTC, which considers the effect of pyrolysis, oxidation, and phase change on the material removal, is limited.

The mechanism of the high-power CW laser resistance of the filled SPTC is the main concern in this study. A series of experiments on the analysis of the ablation residue are conducted to reveal the detailed enhancing mechanism of the filled ablative material to the SPTC. Then, the process of laser heating, pyrolysis and phase change are investigated by simulations performed with a 3D FEM model. The related parameters used in the numerical model are obtained by the thermal gravity analysis (TGA) and differential scanning calorimetry (DSC)

experiment. The precision of the present model is verified by comparing the numerical results with those from the experiment. Finally, the evolution of the laser ablation process, pyrolysis effect and the laser resistance mechanism of the filled SPTC are obtained according to the present model.

2. Experimental observations and ablation mechanisms

2.1. Laser ablation experiments

As shown in Fig. 1(b), the fabricated filled SPTC consists of two thin facesheets and the 3D pyramidal truss cores, which are both made from 304 stainless steel. The void space of the truss core was filled with the compound of silicone resin and carbon powder. The component of silicone resin matrix is polydimethylsiloxane (PDMS). The thickness of the facesheets and the truss core are 0.9 and 7.0 mm, respectively. The size of the specimen is 50 mm × 50 mm.

The laser ablation experiments were tested in a natural convection environment. A 1.07 μm fiber laser with a power of 1000 W was used to irradiate the specimen. The laser spot diameter was fixed at 10 mm. The full-field temperature distribution and ablation process of back surface were measured by a thermal infrared camera. The back-surface temperature histories of structures with different configurations are shown in Fig. 2. This figure shows that, compared with the monolithic plate, the laser resistance of the SPTC, especially that filled with ablative materials is considerably improved.

2.2. Characterization of the filled ablative material

The fabricated filled SPTC is shown in Fig. 3(a), and one of typical melt-through specimen is presented in Fig. 3(b). Some white ablation products were observed around the ablation hole. Several experiments on filler material, which include FTIR and SEM–EDS analysis, were conducted to understand the ablation process. Three kinds of samples were tested: virgin filler material, and black and white ablative residue. Sampling positions are marked by red arrows in Fig. 3.

2.2.1. FTIR analysis

Components of virgin filled ablative material and the white ablation residue were measured by Fourier transform infrared spectroscopy (FTIR) analysis, as shown in Fig. 4. The comparison of the two results reveals the conversion of the ablative material ablation process.

The red line is the FTIR of the virgin material, which is PDMS. The doublet at 1023 cm^{-1} and 1095 cm^{-1} are associated with the stretching of Si–O bond. Meanwhile, other peaks are assigned to the vibrations of hydrocarbon groups, including CH$_2$ wagging at 1261 cm^{-1}, C–H stretching at 2963 cm^{-1}, and Si-CH$_3$ stretching at
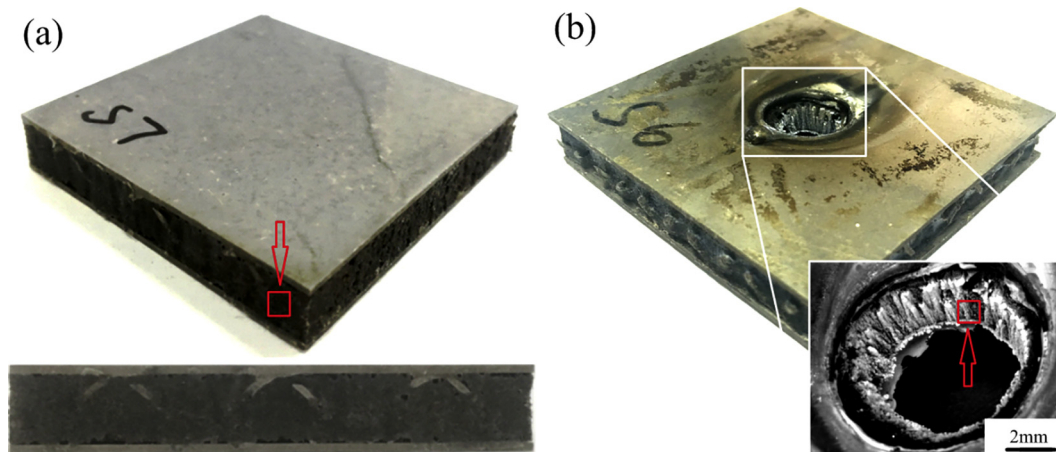
Fig. 3. Experimental samples and their sampling positions: (a) The filled SPTC. (b) The filled SPTC with ablation hole.
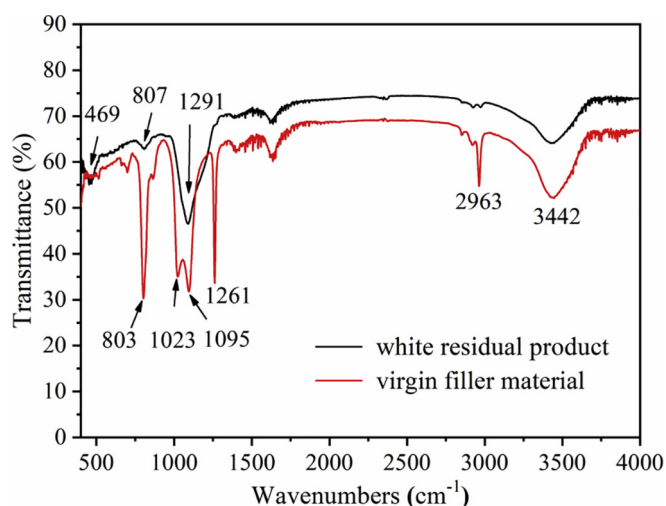

Fig. 4. FT-IR results of virgin filler material and white ablation residue.

803 cm^{-1}, etc. The black solid line is the FTIR of the ablation residue with white color. The evident peak at 1091 cm^{-1} and the two peaks at 807 cm^{-1} and 469 cm^{-1} are associated with the stretching of Si–O bond. Consequently, it can be demonstrated that the main component of white ablation residue is silicon dioxide. The peak at 3442 cm^{-1} suggests the Si–OH bond.

The comparison of the two lines indicates that the peaks of hydrocarbon groups in virgin filler material are nearly removed after the laser ablation process, and the doublet of Si–O bond is converted to an evident singlet. This finding suggests that the filler material is nearly degraded, thereby leaving only silicon dioxide.

2.2.2. SEM and EDS analysis

Scanning electron microscope (SEM) and energy dispersive spectrometer (EDS) of the virgin material and the ablation residue with black and white color are shown in Figs. 5 and 6, respectively. As shown in Fig. 5(a) and (b), areas A and B are the conductive tape and the resin slice, respectively. Uniformly distributed spherical particles with diameters of 100–200 μm in area C are the carbon powder. The principal element of these spherical particles in Fig. 5(a) and (b) is carbon. Small elements of Na, Cl, and P, which come from the additive used in the preparation process of filler material, are also observed. Fig. 5(c) and

(d) shows the microstructure of the white ablation residue. The loose and irregular structure indicates that it has undergone a solidification process in the laser ablation. Fig. 5(e) and (f) indicates the black residue comprising clusters of particle substance with approximately 2–3 μm in diameter. These small unordered stacked spherical particles are amorphous carbon. The finding suggests that the filler material has undergone complex thermo-chemical process during laser ablation, and the carbon powder is no longer in the steady initial state. The comparison of two ablation residues demonstrates their difference.

Compositions and contents of the virgin and ablation residue according to the EDS are presented in Table 1. Approximately 90% element of the black residue is carbon, which indicates that the ablative material nearby the laser irradiation area has nearly changed into carbon. The carbon is mainly derived from the pyrolytic of silicone resin and the filled carbon powder. The increase in silicon element and decrease in oxygen element between the virgin material and white ablation residue reveal the pyrolysis process of filler material. Elements of Fe, Cr, and Ni are obtained from the melting sandwich plates. Notably, the proportion of Si and O elements in white ablative residue is less than 1:2, indicating the existence of SiC. The possible reaction is as follows:

$$SiO_2(s) + 3C(s) \rightarrow SiC(s) + CO(g)$$
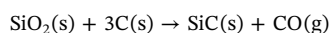
2.3. Ablation mechanisms of the filled ablative material

The ablative material experiences physical and chemical reactions, including pyrolysis, oxidation and phase change, during the ablation process. With increasing temperature, silica in the pyrolytic products turns into gases and gradually re-solidifies on the surface of the ablation hole. The major ingredient of the ablative residue around the ablation hole is residual carbon.

As shown in Fig. 7, the filler material can be divided into the following three layers: char layer, degradation layer and virgin layer. These layers play different roles on laser resistance, based on their thermochemical and thermophysical properties.

The major components for char layer are simplified as SiO$_2$, residual carbon and a little SiC. SiO$_2$ is generated by the oxidation of Si–O groups. The temperature variation in char layer is above 1800 °C. SiO$_2$ in this layer vaporizes, leaving only the carbon element. The phase change of SiO$_2$ and carbon absorbs a considerable amount of heat energy generated by the laser irradiation. For degradation layer, the main components are porous pyrolysis products without oxidation. The temperature of degradation layer is from 340 °C to over 1000 °C. This
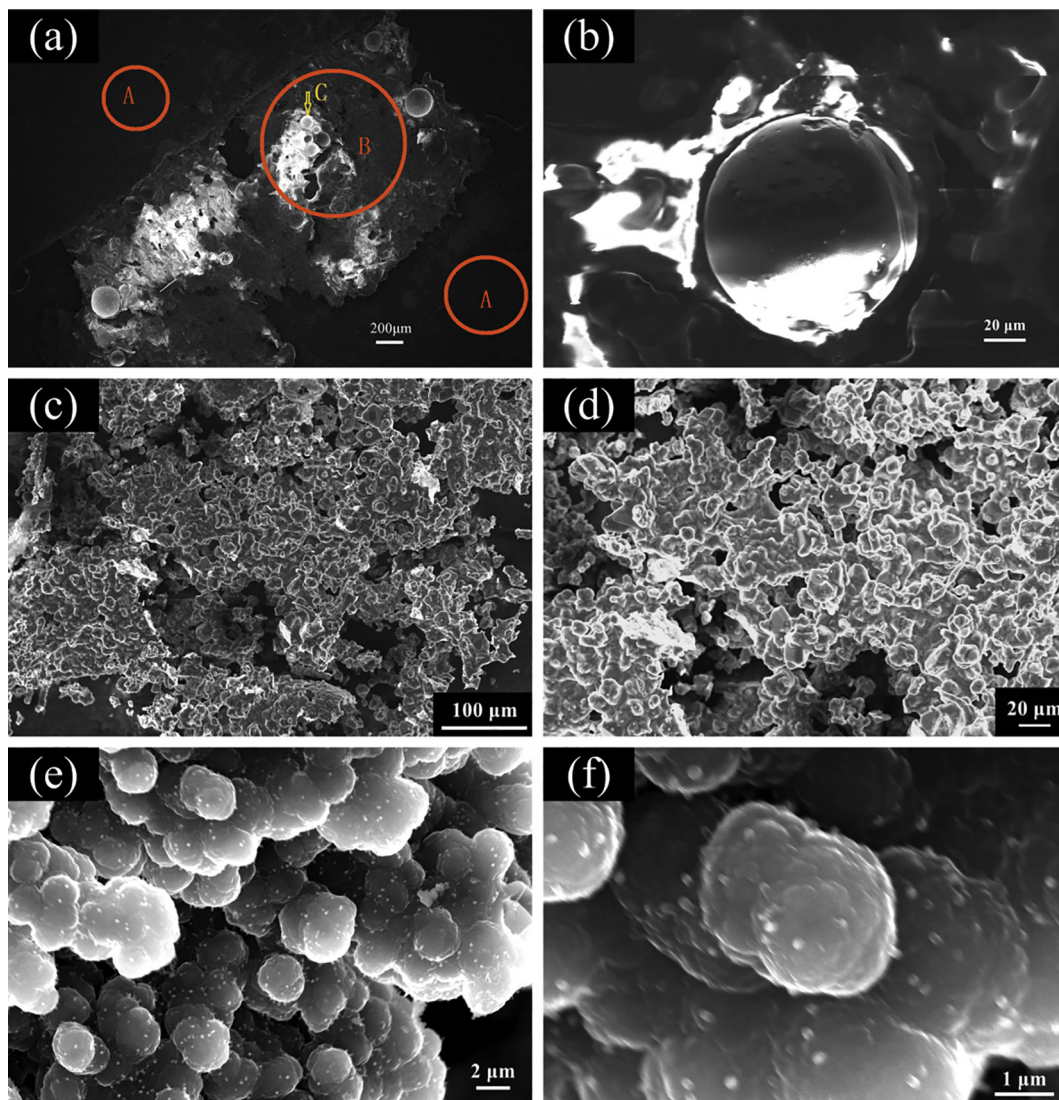
Fig. 5. SEM morphology of samples: (a) virgin filler material, region A is the conductive tape, region B is the matrix slice, region C is a typical spherical particle region, (b) spherical particle (region C) of carbon powder in virgin filler material, (c–d) white residue product, (e–f) black residue product.

layer can also be regarded as a thermal insulation layer due to the low thermal conductivity of the porous pyrolysis. The pyrolytic process, as an endothermic reaction, enhances the laser resistance capability of the filler material. For virgin layer, the main component is the filled carbon powder reinforced silicone resin composite. The temperature of this layer ranges from ambient temperature to 340 °C. The virgin layer also has an insulating effect on the high-temperature region of upper layers due to its low thermal conductivity.

3. Numerical modeling

The numerical model based on the commercial software ANSYS was developed to investigate the laser ablation process. Thermal response region is relatively small compared with that of the entire filled SPTC due to the low heat conductivity coefficient of the filler material. Therefore, as shown in Fig. 8, a one quarter FEM model is used and the size of the SPTC is $15 \times 15 \, mm^2$ to reduce the amount of calculations.

The thickness of the facesheet and the truss core are 0.9 and 7 mm respectively. For simplicity, the following assumptions are made in the numerical model:

(1) The heat conduction of truss cores is ignored.
(2) Surface tension of the molten metal in the facesheet is disregarded.
(3) The laser absorption coefficient is constant in the ablation process.
(4) The virgin ablative materials and pyrolysis products are homogeneous and isotropic. The physical parameters of corresponding pure substances are used.
(5) The effect of diffusion and convection of pyrolysis gas flow in solid phase is neglected.

The computational mass and heat transfer model are shown in Fig. 9. Mass transfer during laser ablation process, including pyrolysis, oxidation, sublimaton, is complex. Different mass transfer processes are accompanied by the temperature change of SPTC.
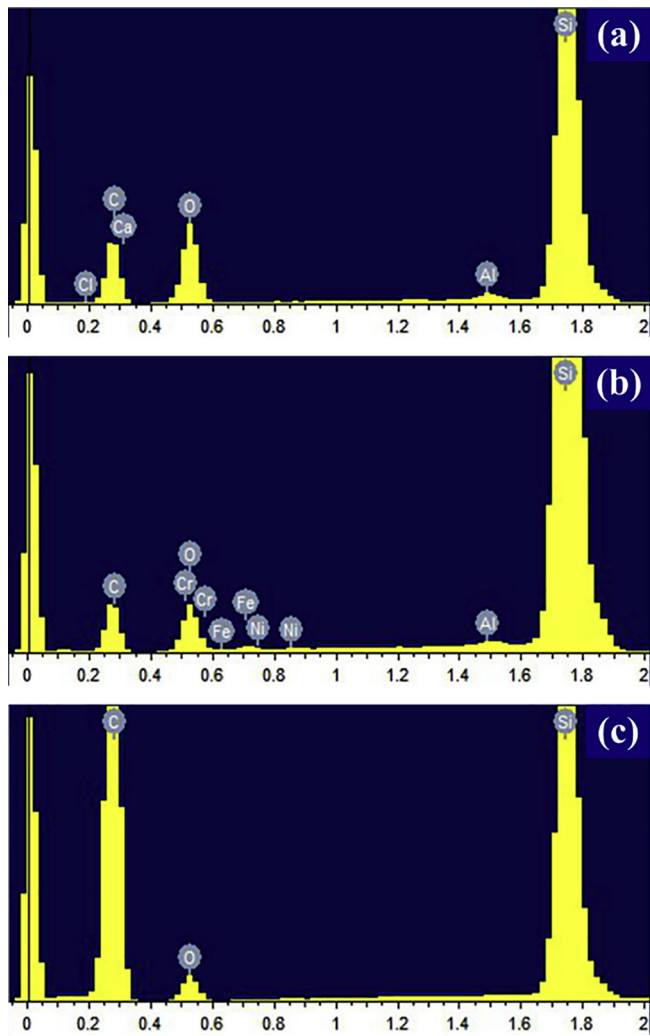
Fig. 6. EDS analysis results: (a) virgin filler material, (b) white residue product, (c) black residue product.

Table 1
Atomic percentages results of the component evaluation.

Samples	C%	Si%	O%	Total%	Other elements
Virgin filler material	55.80	12.63	31.06	99.49	Al, Ca, Cl
White residue product	57.04	24.81	16.55	98.4	Al, Fe, Cr, Ni
Black residue product	88.28	5.04	6.68	100	[spsslashback]

3.1. Pyrolysis model

As shown in Fig. 10, the pyrolysis process of ablative material was analyzed by TGA and DSC experiment in nitrogen and air environment, respectively, with a heating rate of 10 °C/min. The effect of oxidation on the ablation process can be obtained by comparing the two experiments. The pyrolysis process occurred in the temperature region from 340 °C (with 5% mass loss) to 680 °C. The percentage of residual mass in air is 35.4% and that in nitrogen environment is 29.7%. The mass difference mainly comes from the contribution of oxygen element in the process of oxidation from Si–O to SiO_2. Accordingly, the calculated mass ratio of residual carbon is approximately 17.8% after pyrolysis.

The residual mass is nearly constant in the nitrogen and air environment when pyrolysis of the silicone resin is completed. This finding is due to the protective effect of the newly formed SiO_2 in the sample surface, stopping the oxidation of the inside residual carbon.

The total heat of pyrolysis and oxidation process can be obtained by the DSC results shown in Fig. 11. The absorbing heat Q during the pyrolysis process is calculated via the integration of the shadow area in Fig. 11 [33], which is −3964.8 J/g.

The heat generation rate and thermophysical properties are governed by the kinetic model of pyrolysis. The empirical kinetic model is based on Arrhenius relation [34]. The mass loss reaction, which is assumed to be irreversible, can be described as:

$$-\frac{\partial(m/m_0)}{\partial t} = k\left(\frac{m-m_r}{m_0}\right)^n,$$
(1)

where the specific rate k is expressed by the Arrhenius relation:

$$k = -A\exp\left(-\frac{E}{RT}\right)$$
(2)

combining Eqs. (1) and (2),

$$\frac{\partial(m/m_0)}{\partial t} = -A\left(\frac{m-m_r}{m_0}\right)^n \exp\left(-\frac{E}{RT}\right),$$
(3)

where A is frequency factor; E is activation energy; which is a kinetic parameter; n is order of the reaction; m_0 is the initial mass of the material; m_r is the residual mass of the material; m is the mass at current time; T is the current temperature; R is ideal gas constant. The directed-solution method [34] is employed to obtain parameter values of Eq. (3) from TG and DTG curves (Fig. 10(a)). The pyrolysis process has two main steps. The kinetic parameters are shown in Table 2. In addition, thermophysical properties of the filler material change as functions of mass loss, which is governed by the kinetic model.

3.2. Oxidation model

The heat released in the oxidation process, which is 7155.2 J/g, corresponds to the enclosed area between the heat flow in nitrogen and air environment shown in Fig. 11. The heat flux generated by the oxidation of the residual carbon and the filled carbon powder are obtained based on the following assumptions.

(1) Oxidation only occurs at the completely pyrolyzed surface layer of ablative materials.
(2) The diffusion rate of oxygen determines the oxidation kinetics because temperature of oxidation reaction region is over 1000 °C [35].
(3) Heat absorption in the generation reaction of SiC is neglected.

The reaction rate of oxidation is described by Fick's law

$$N_{A,x} = \frac{D_{AB}A}{L}(C_{A,s2}-C_{A,s1})$$
(4)

where D_{AB} is binary diffusion coefficient, $C_{A,s1}$ and $C_{A,s2}$ are molar concentrations. The molar concentration of oxygen in air is 0.00969 kmol/m³. The order of binary diffusion coefficient in the simulation is 10^{-5}, which is equal to that of oxygen at air atmosphere because the char layer is loose and sufficiently porous. The calculated heat flux density of oxidation is approximately 50% of laser power density. Therefore, oxidation cannot be neglected in the simulation of laser ablation model.
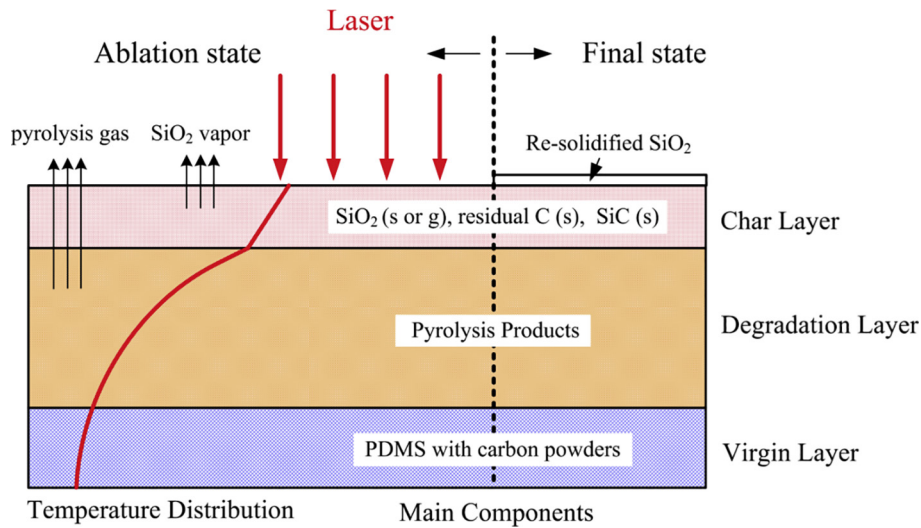
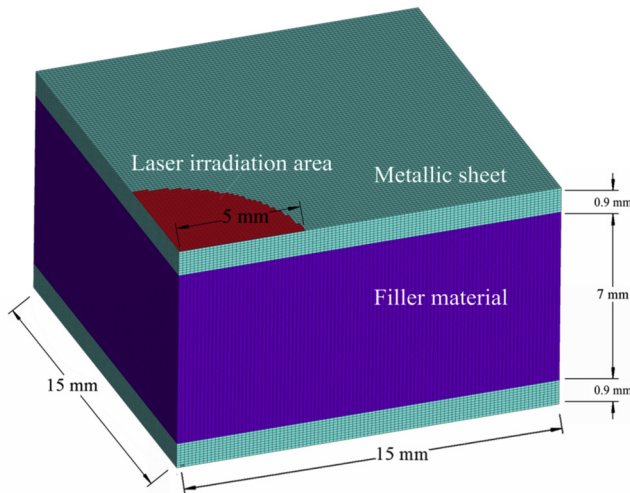**Fig. 7.** Schematic diagram of filler material in three layers.

Fig. 8. One-quarter finite element model of SPTC filled with silicone resin (PDMS).

3.3. Phase change model

Phase change process of silica and carbon is solved by assigning elements with the material property of enthalpy instead of heat capacity. This method is efficient to describe boiling and condensation, or melting and solidification in ANSYS [36].

The enthalpy for the phase change system is in the following form

$$H(T) = \begin{cases} \rho C_s T, & T < T_s; \\ H_s + \rho C^*(T - T_s), & T_s < T < T_l; \\ H_l + \rho C_l(T - T_l), & T > T_l; \end{cases} \quad (5)$$

$$C^* = \left(\frac{C_s + C_l}{2} \right) + \frac{L}{T_l - T_s} \quad (6)$$

where C and ρ are mass specific heat and density of the material respectively. The subscript s and l indicate solid and liquid states,

respectively. H_s and H_l are enthalpy values at the beginning and ending temperature of the phase transition region, respectively. Parameters used in Eqs. (5) and (6) are listed in Table 3.

Thermophysical properties of materials are given in Table 3, and the calculation data used in the numerical model are provided in Table 4.

4. Numerical results and discussion

4.1. Model verification

The comparison of the spot center temperature histories in the back surface (Fig. 12) shows that the thermal response time and the temperature below 500 °C agree with those from the experiments. The overvaluation of temperature exceeding 500 °C is mainly due to the imprecision of thermophysical properties of the mixture containing the molten facesheet and the residual ablative material. In addition, the constant emissivity assumption increases the calculated temperature.

The increase in the carbon power content delays the thermal response and failure time of the filled SPTC with the same density. This finding reveals that the absorption capacity of the laser heating of the carbon powder with high latent heat is crucial in enhancing the laser resistance of the SPTC. Fig. 13 compares the full-field temperature of the back surface, and a basic agreement can be found. Moreover, the numerical model cannot simulate surface tension effect of liquid metal. Therefore, the failure time in the numerical model is a slightly shorter than that from the experiment.

4.2. Evolution of laser ablation process

Fig. 14 shows the evolution of the laser ablation process of the filled SPTC. The bottom of the ablation hole for the ablative material is nearly plane, as shown in Fig. 14(c) and (d), and the bottom of facesheet is an upside-down cone, as shown in n in Fig. 14(b), (e), and (f). This finding can be attributed to the evidently lower inward diffusion velocity of the ablative material than that of the metallic material. The heat-affected zone in the back surface of the SPTC is only approximately 50% of the front surface, as shown in Fig. 14(f).

As shown in Fig. 14(e), the char layer of filler material still exists
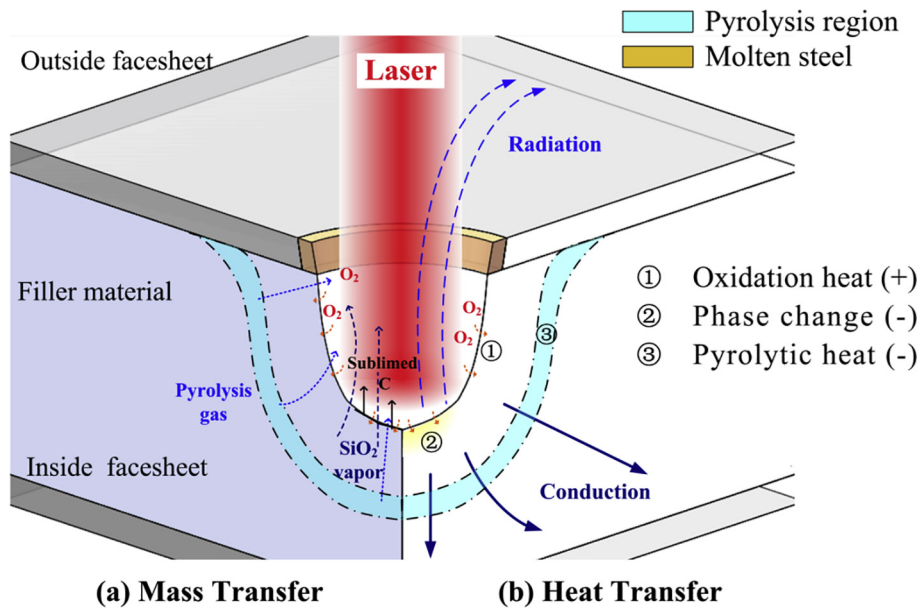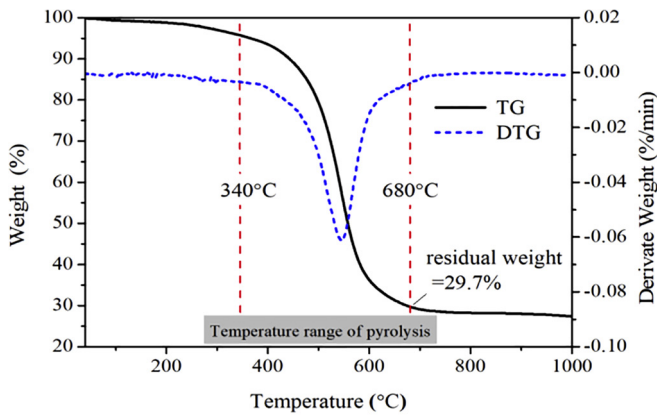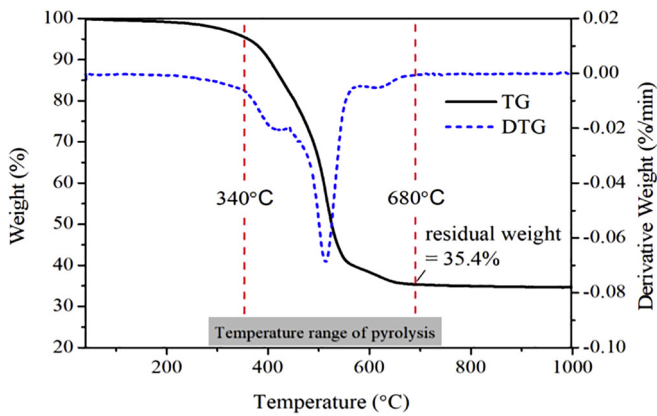
Fig. 9. Mass and heat transfer of filled SPTC during laser ablation process.

(a) At nitrogen atmosphere

(b) At air atmosphere

Fig. 10. TG/DTG results of filler material: (a) nitrogen atmosphere, with a mass percentage of 29.7%; (b) air atmosphere, with a mass percentage of 35.4%.

Fig. 11. DSC analysis of filler materials in nitrogen and in air. Degradation heat is -3964.8 J/g, corresponding the shadow area (minus sign stands for absorbing heat). Oxidation heat of pyrolysis products is 7155.2 J/g, corresponding the enclosed area between two heat flow curves.

Table 2
Parameters of the Arrhenius relation.

	n_i	$\ln A_i$ (s^{-1})	$-E_i/R$ (K^{-1})	Initial temperature (°C)	Final temperature (°C)
First step	0	9.55	8359.5	340	545
Second step	2.7	39.88	31322.1	545	680

eliminated due to the high temperature of residual products.

4.3. Effects of pyrolysis

The comparison of the cross-sectional view of the ablation morphology from the experiment with that from the numerical model is shown in Fig. 15. Materials in regions (I) and (II) are the virgin filler

when the temperature of back facesheet reaches the melting point. This result demonstrates that the filled SPTC loses its laser resistance when the virgin layer disappears. The protection of the ablative filler is then
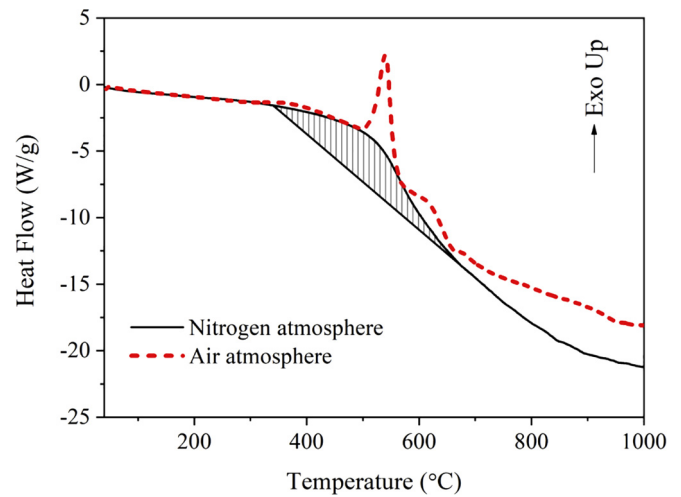
Table 3

Thermo-physical properties of the pure materials under ambient conditions [37,38].

Property	AISI 304	PDMS	SiO$_2$	Carbon
Density (kg m^{-3})	7900	1100	2334	2200
Thermal conductivity (W m^{-1} K^{-1})	14.9	0.28	1.38	1.60
Specific heat (J kg^{-1} K^{-1})	477	1400	745	709
Melting point/sublimation point (°C)	1200	[spsslashback]	1722	3825
Latent heat ($\times 10^6$ J kg^{-1})	0.246	[spsslashback]	12.69	59.45
Empirical phase change temperature range (°C)	100	[spsslashback]	200	400

Table 4

Parameters used in numerical model.

Parameters	Value
Laser power Q_{laser} (W)	1000
Laser beam radius (mm)	5
Laser absorption coefficient of metal material	0.65
Laser absorption coefficient of filler material	0.78
Stefan-Boltzmann constant ($\times 10^{-8}$ W m^{-2} K^{-4})	5.67
Ambient temperature T_0 (°C)	20
Surface of emissivity	0.8

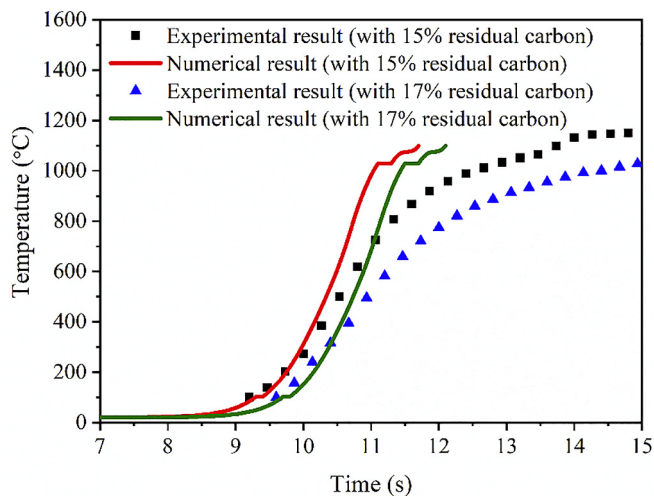**Fig. 12.** Numerical results of temperature history at the center point of back surface, compared with corresponding experimental data.
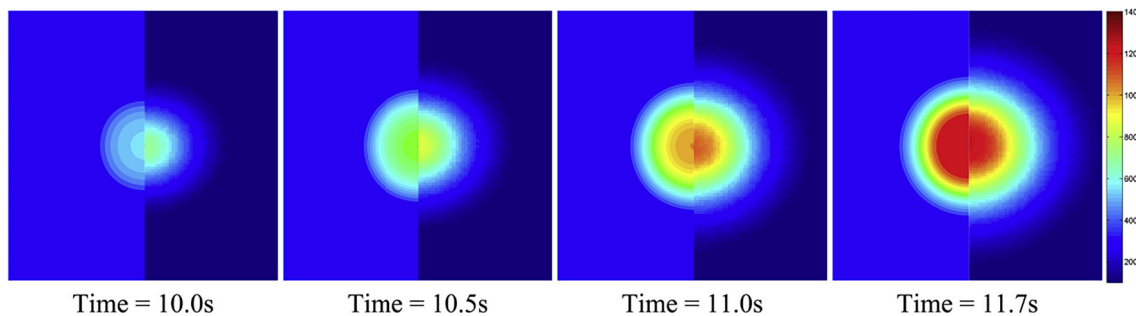
material and pyrolysis residue, respectively. The length of region (II) at the interface with front plate l_1 and the width of vertical region are approximately 5.8 and 3.2 mm, respectively, while those of the numerical model are 4.9 and 2.2 mm, respectively. The difference in the size of the pyrolysis shape is mainly due to the heat diffusion effect of the high-temperature region after laser irradiation. Ablation hole in region (III) is characterized by massive damage in the outside surface and minimal inside, reducing laser damages to the inner equipment. An evident boundary can be seen in the exposed images, as shown in Fig. 15(c).

Fig. 16 shows the effect of pyrolytic heat in the degradation layer on laser resistance of the filled SPTC. The absorption of the laser energy by the pyrolysis process delays the time it takes for the high-temperature influence to reach the back surface. The melt-through time is approximately 0.5 s less when the pyrolytic heat is not considered.

4.4. Laser resistance of filled SPTC

For structures exposed to an external high-speed air flow or a substantial pressure difference between the front and back surfaces, delaying the temperature of the back surface reaching the melting point is the main objective.

Before the front facesheet is melted through, the ablative filler material increases the thermal resistance of the truss core by insulating the thermal radiation between the two facesheets. Therefore, compared with the unfilled SPTC, additional heat energy is stored in the front facesheet. After the destruction of the front facesheet, the ablative material also prevents the direct laser irradiation on the back facesheet. During the laser ablation process, the typical spot center temperature distribution along the thickness direction at laser irradiation time is shown in Fig. 17. The char layer, which ranges from the melting point of SiO$_2$ to the sublimating point of carbon, experienced a large temperature difference due to the low heat capacity of porous pyrolysis residue. The temperature decreases in region (b) due to the heat absorption by the phase change of SiO$_2$. Moreover, the insulation effect of degradation layer delays the heat conduction to the inside surface, thereby, rapidly decreasing the temperature. Consequently, the temperature of virgin layer in region (d) and back facesheet in region (e) is nearly unchanged. Therefore, filling the SPTC with ablative materials can increase its laser resistance.

The thickness of virgin layer and the ablation boundary decreases linearly, as shown in Fig. 18. The virgin layer thickness reduces to zero at approximately 9.1 s. The sudden drop of ablation boundary at 11.0 s indicates the failure of back plate. Notably, the temperature of back plate starts to rise when the virgin layer disappears. This finding indicates the thermal insulation of virgin layer. The subsequent increase in temperature is due to the conduction of degradation and char layers.
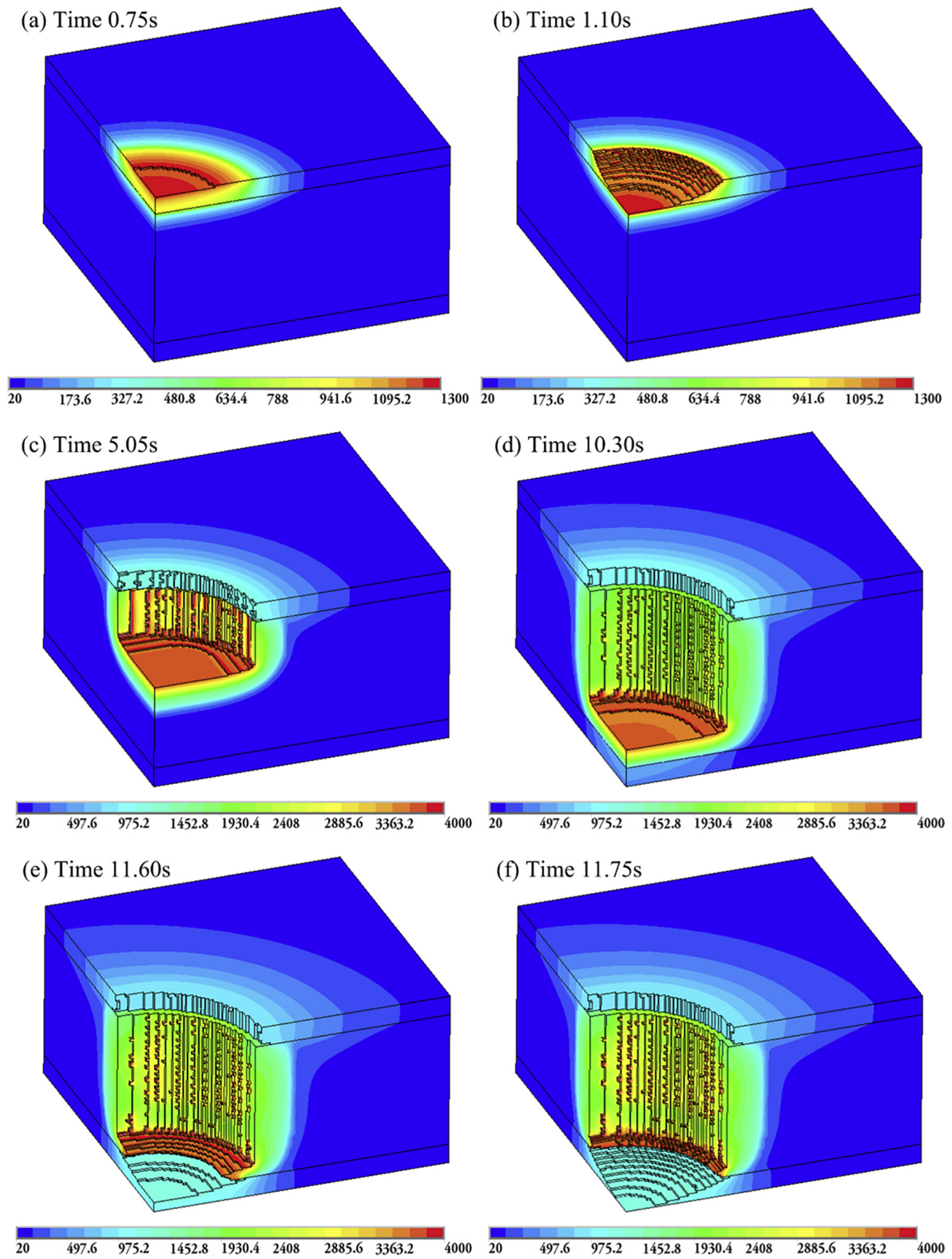

Fig. 13. Comparisons of temperature distribution of back surface. On the left: numerical results, on the right: experimental results.

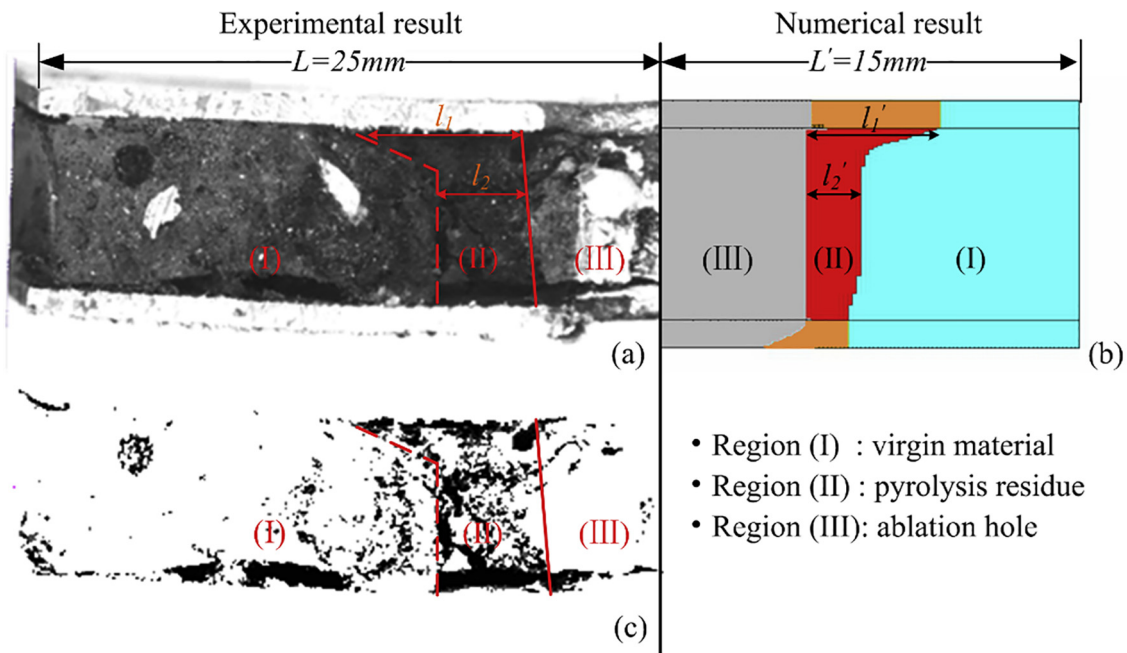**Fig. 14.** Evolution of the laser ablation process.

Fig. 15. Profile comparison of final state after ablation process: (a) experimental result, (b) numerical result, (c) over-exposed image of experimental result (showing the region of pyrolysis residue more intuitively).
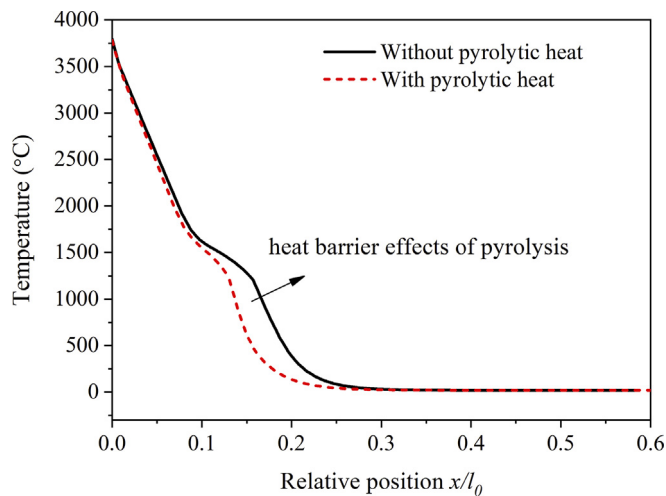

Fig. 16. Comparison of laser irradiation center temperature distributions along Z-direction (laser irradiation time is 5.2 s) with consideration of pyrolysis or not.
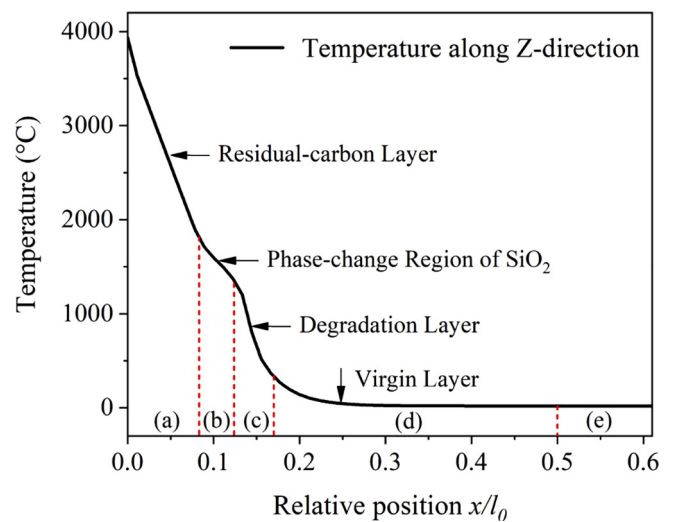

Fig. 17. Typical laser irradiation center temperature distribution along thickness direction (laser irradiation time is 5.2 s). Region (a)–(e) represent different layers of residue material. Region (e) is backplate of sandwich structure. Total thickness l_0 is 0.9 cm.

5. Conclusions

The laser resistance mechanism of silicone resin composites filled SPTC is experimentally and numerically investigated in the present paper. A series of experiments on microstructures of the filler material is conducted to reveal the laser ablation process. A 3D FEM model considering the process of laser heating, pyrolysis and phase change is developed to obtain the detailed laser resistance mechanism of the filled SPTC. TGA and DSC experiments are performed to find the related parameters used in the numerical model. The filler material is sub-divided into three layers during the laser ablation process. The three layers with different roles on laser resistance experience various thermal physical and chemical processes. Combined effects of endothermic process by the phase change and the pyrolysis, along with thermal insulation by virgin and degradation layers, delay the time in which high heat flux reaches the back surface of the filled sandwich structures.
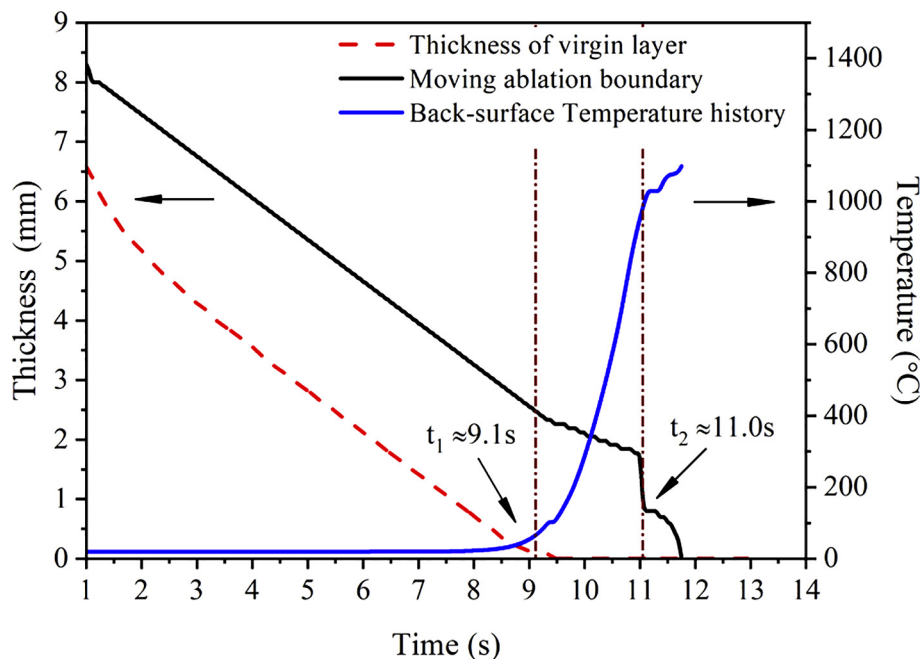
Fig. 18. Evolution of virgin layer and ablation boundary, comparing with the temperature history of back surface of SPTC.

Acknowledgements

References

[1] Deshpande VS, Fleck NA. Collapse of truss core sandwich beams in 3-point bending. Int J Solids Struct 2001;38:6275–305.

[2] Yuan W, Song H, Wang X, Huang C. Experimental investigation on thermal buckling behavior of truss-core sandwich panels. AIAA J 2015;53:948–57.

[3] Clough EC, Jie E, Eckel ZC, Ro CJ, Schaedler TA. Mechanical performance of hollow tetrahedral truss cores. Int J Solids Struct 2016;91:115–26.

[4] Wadley HNG. Multifunctional periodic cellular metals. Philos Trans 2006;364:31.

[5] Gibson RF. A review of recent research on mechanics of multifunctional composite materials and structures. Compos Struct 2010;92:2793–810.

[6] D'Mello RJ, Waas AM. Inplane crush response and energy absorption of circular cell honeycomb filled with elastomer. Compos Struct 2013;106:491–501.

[7] Wei K. Design and analysis of integrated thermal protection system based on lightweight C/SiC pyramidal lattice core sandwich panel. Mater Des 2016;111:435–44.

[8] Lu T, Valdevit L, Evans A. Active cooling by metallic sandwich structures with periodic cores. Prog Mater Sci 2005;50:789–815.

[9] Martinez OA, Sharma A, Sankar BV, Haftka RT, Blosser ML. Thermal force and moment determination of an integrated thermal protection system. AIAA J 2010;48:119–28.

[10] Ma Y, Xu B, Chen M, He R, Wen W, Cheng T, et al. Optimization design of built-up thermal protection system based on validation of corrugated core homogenization. Appl Therm Eng 2017;115:491–500.

[11] Ashby MF, Evans T, Fleck NA, Hutchinson J, Wadley H, Gibson L. Metal Foams: A Design Guide. Elsevier; 2000.

[12] Radford D, Fleck N, Deshpande V. The response of clamped sandwich beams subjected to shock loading. Int J Impact Eng 2006;32:968–87.

[13] Yungwirth CJ, Radford DD, Aronson M, Wadley HN. Experiment assessment of the ballistic response of composite pyramidal lattice truss structures. Compos B Eng 2008;39:556–69.

[14] Yan L, Yu B, Han B, Chen C, Zhang Q, Lu T. Compressive strength and energy absorption of sandwich panels with aluminum foam-filled corrugated cores. Compos Sci Technol 2013;86:142–8.

[15] Yuan W, Wang J, Song H, Ma T, Wu W, Li J, et al. High-power laser resistance of filled sandwich panel with truss core: an experimental study. Compos Struct 2018.

[16] Chen Y, Bai T, Dong N, Fan F, Zhang S, Zhuang X, et al. Graphene and its derivatives for laser protection. Prog Mater Sci 2016;84:118–57.

[17] Li J, Guan ZW, Zhang YZ, Wang Y, Wang ZY. Laser ablation resistance behavior of organosilicone composite coating on various substrates. Materials science forum. Trans Tech Publ; 2014. p. 461–5.

[18] Muric BD, Pantelic DV, Vasiljevic DM, Savic-Sevic SN, Jelenkovic BM. Application of tot'hema eosin sensitized gelatin as a potential eye protection filter against direct laser radiation. Curr Appl Phys 2016;16:57–62.

[19] Zhang D, He H, Zhao Y, Li D, Fan Z. Method for characterization of repetitive frequency laser resistance of optical coatings. Appl Opt 2009;48:2860–4.

[20] Natali M, Kenny JM, Torre L. Science and technology of polymeric ablative materials for thermal protection systems and propulsion devices: a review. Prog Mater Sci 2016;84:192–275.

[21] Cohen LS, Couch HT, Murrin TA. Performance of ablative materials in ramjet environments. Heat transfer with thermal control applications. Cambridge, Massachusetts: The MIT Press; 1975.

[22] Yamada S, Serizawa C, Kato K, Yamada S, Serizawa C, Kato K. Thermal and ablative properties of silicone insulation. 33rd joint propulsion conference and exhibit. 1997. p. 3259.

[23] Kim ES, Kim EJ, Shim JH, Yoon JS. Thermal stability and ablation properties of silicone rubber composites. J Appl Polym Sci 2008;110:1263–70.

[24] Tran HK, Johnson C, Rasky D, Hui F, Hsu M. Silicone impregnated reusable ceramic ablators for Mars follow-on missions. AIAA Paper 1996;1819:1996.

[25] Strauss EL. Superlight ablative systems for Mars lander thermal protection. Atmosphere 1967;1005:7.

[26] Bartlett EP, Anderson LW, Curry DM. An evaluation of ablation mechanisms for the Apollo heat shield material. J Spacecraf Rock 1971;8:463–9.

[27] Webster F. Liquid fueled integral rocket ramjet technology review. AIAA Paper 1978;78.

[28] Beall G, Shirin Z, Harris S, Wooten M, Smith C, Bray A. Development of an ablative insulation material for ramjet applications. J Spacecraf Rock 2004;41:1068–71.

[29] Vignoles GL, Lachaud J, Aspa Y, Goyhénèche JM. Ablation of carbon-based materials: multiscale roughness modelling. Compos Sci Technol 2009;69:1470–7.

[30] Lachaud J, Aspa Y, Vignoles GL. Analytical modeling of the steady state ablation of a 3D C/C composite. Int J Heat Mass Transf 2008;51:2614–27.

[31] Newnham P, Abrate S. Finite element analysis of heat transfer in anisotropic solids: application to manufacturing problems. J Reinforced Plast Compos 1993;12:854–64.

[32] Negarestani R, Sundar M, Sheikh M, Mativenga P, Li L, Li Z, et al. Numerical simulation of laser machining of carbon-fibre-reinforced composites. Proc Inst Mech Eng Part B J Eng Manuf 2010;224:1017–27.

[33] Torre L, Kenny J, Maffezzoli A. Degradation behaviour of a composite material for thermal protection systems Part I-Experimental characterization. J Mater Sci 1998;33:3137–43.

[34] Nelson JB. Determination of kinetic parameters of six ablation polymers by thermogravimetric. Analysis 1967.

[35] Deal BE, Grove A. General relationship for the thermal oxidation of silicon. J Appl Phys 1965;36:3770–8.

[36] Theory Ansys I. Reference for the mechanical APDL and mechanical Applications. Southpointe Release 2009;12.

[37] Bergman TL. Incropera FP. Fundamentals of heat and mass transfer. John Wiley & Sons; 2011.

[38] Haynes WM. CRC handbook of chemistry and physics. CRC Press; 2014.